arXiv:1504.04040v1 [cond-mat.mes-hall] 15 Apr 2015

Triangular lattice exciton model

Daniel Gunlycke* and Frank Tseng†
Naval Research Laboratory, Washington, D.C. 20375, USA

We present a minimalistic equilateral triangular lattice model, from which we derive electron and exciton band structures for semiconducting transition-metal dichalcogenides. With explicit consideration of the exchange interaction, this model is appropriate across the spectrum from Wannier to Frenkel excitons. The single-particle contributions are obtained from a nearest-neighbor tight-binding model parameterized using the effective mass and spin-orbit coupling. The solutions to the characteristic equation, computed in direct space, are in qualitative agreement with first-principles calculations and highlight the inadequacy of the two-dimensional hydrogen model to describe the lowest-energy exciton bands. The model confirms the lack of subshell degeneracy and shows that the A-B exciton split depends on the electrostatic environment as well as the spin-orbit interaction.

PACS numbers: 73.22.Dj, 73.22.Lp, 78.67.-n, 78.67.Bf

I. INTRODUCTION

It is well known that the electronic properties of a crystal depend critically on its crystal structure. Yet, the lattice is usually absent from descriptions of low-energy electronic excitations in pristine semiconducting or insulating crystals. The reason the lattice can often be ignored is that these excitations generate bound electron and hole pairs, known as excitons, that are typically either confined to single sites or span regions much larger than the relevant lattice constant. The energies of the former site-confined excitons can be estimated by the energetics of the excited site and an "exchange energy" from neighboring sites.[1] These excitons have been named after Frenkel and can be found in e.g. molecular solids. The second type of excitons can be described by the hydrogen model adapted for excitons[2] and are usually referred to as Wannier–Mott excitons and can be found in semiconductors with large permittivities and dispersive charge carriers.

Lattice effects could be important, however, in the description of excitons in semiconducting transition metal dichalcogenides such as molybdenum disulfide (MoS_2). These lubricants, investigated in the 1960s,[3–5] have received renewed interest after the isolation of individual layers[6] and the demonstration that the monolayers, unlike their bulk counterpart, are direct gap[7,8] semiconductors. An estimate for the separation of the electron and hole in a two-dimensional (2D) semiconductor is the ground state radial expectation value of the 2D hydrogen model[9,10] for excitons $\langle r\rangle_{1s} \sim 0.09\varepsilon_r$ nm, where ε_r is the relative permittivity. Relative permittivities are expected to be quite small in 2D materials,[11–13] and for $\varepsilon_r \lesssim 3.5$, the expectation value $\langle r\rangle_{1s}$ becomes smaller than the lattice constant a in these materials, which necessitates atomistic treatment. The exciton binding energy provides another rough measure of the degree to which the excitons are confined. Unfortunately, there is no conclusive band edge feature in the optical spectroscopy data, which has resulted in different interpretations of observed spectroscopic features.[3,14–19] Furthermore, band gap predictions based on density functional theory depends significantly on calculation details.[12,16,20–27] Photoconductivity[3,28] and scanning tunneling spectroscopy[29] data suggests a binding energy of at least 0.5 eV, providing further indication that the exciton radius is of the order of the lattice constant.

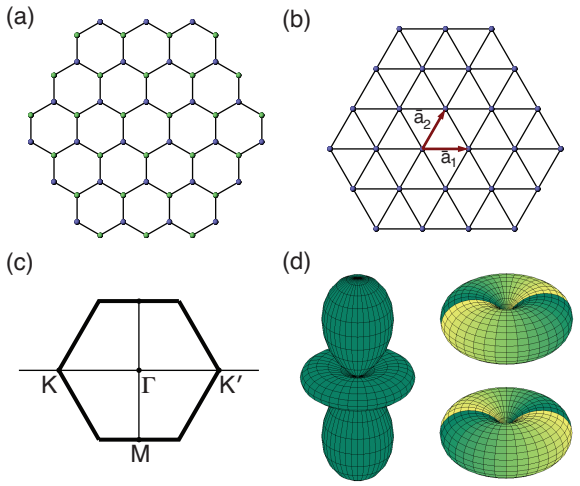

FIG. 1. (Color online) (a) Top view of the hexagonal-tiled structure of trigonal prismatic monolayer transition metal dichalcogenides. (b) The transition-metal sites form a triangular-tiled structure that exposes the underlying equilateral triangular lattice. (c) First Brillouin zone of the equilateral triangular lattice with symmetry points Γ, K, K′, and M. (d) The conduction and valence band d-orbitals at K and K′ have magnitudes that are azimuthally symmetric.

We present a minimalistic exciton model, which we refer to as the triangular lattice exciton (3-ALE) model. This model accounts for both the exchange and spin-orbit interactions and the equilateral triangular lattice shown in Fig. 1. A dielectric constant or function is used to account for dielectric polarization. Unlike typical exciton models solving the Bethe-Salpeter equation[30–32] in reciprocal space, we derive a characteristic equation on sparse form in direct space, thus allowing great computational efficiency. This efficiency enables large calculations and hence avoids the convergence challenge for tightly bound electron/hole pairs.[33] The long-range Coulomb interaction in direct space causes no problem for tightly bound electron/hole pairs in transition-metal dichalcogenides. Our model illustrates the breakdown of the 2D hydrogen model for low permittivity through the atomic scale electron-hole separation and the binding energies and oscillator strengths of the lowest exciton states. In addition, the model shows that:

(1) optically allowed exciton states depend sensitively on the shared-site potential, as well as the relative permittivity, (2) the degeneracy within lower shells is broken, and (3) the energy separation between the A and B excitons depends on the electrostatic environment, as well as the spin-orbit coupling.[3]

The 3-ALE model can, as is usually the case for exciton models, be separated into electron and hole contributions and a contribution from their mutual Coulomb interaction. Sections II and III present the single-particle triangular lattice model and the complete 3-ALE model, respectively. Section IV provides conclusions about the 3-ALE model together with suggestions for possible generalizations.

II. TRIANGULAR LATTICE MODEL

Monolayers of trigonal-prismatic transition-metal dichalcogenides have a hexagonal-tiled structure as shown in Fig. 1(a) with trigonal point group symmetry D_{3h}. The bands around the Fermi level are transition metal d-bands[5] with only small contributions from the chalcogenides entering through hybridization,[34–36] which we will herein neglect. This allows us to construct a basis comprised solely by transition-metal sites. Without the chalcogenide sites, we have exposed the equilateral triangular lattice in these crystals shown in Fig. 1(b). This triangular-tiled structure has a point group pseudosymmetry D_{6h}. Pseudosymmetry can be useful, but it is imperative that one exercise caution as pseudosymmetry introduces artificial symmetry, in the present case inversion symmetry.

The triangular lattice is generated by a set of translation vectors $\vec{R}$, which are linear combinations of the lattice vectors $\vec{a}_1 = a\hat{x}$ and $\vec{a}_2 = a(\hat{x} + \sqrt{3}\hat{y})/2$ with a being the lattice constant. We can introduce an electron field on the triangular lattice through the hermitian conjugate of the electron field operator

$$\Psi(\vec{r}) = \sum_{n\sigma\vec{R}} c_{n\sigma\vec{R}}\, \phi_{n\sigma}(\vec{r} - \vec{R}), \tag{1}$$

where $c_{n\sigma\vec{R}}$ is the annihilation operator for an electron in the Wannier orbital[2] $\phi_{n\sigma}(\vec{r} - \vec{R})$ centered on site $\vec{R}$ with $n \in \{c, v\}$ and $\sigma \in \{\pm 1/2\}$ being band and spin indices, respectively. Within the tight-binding approximation, these Wannier orbitals can be viewed as isolated atomic orbitals. The electronic states outside the band gap near the band edges

TABLE I. Transition-metal dichalcogenide parameters provided in units of electron volts, electron mass, and nanometers. The hopping parameter for each material obtained from the effective mass m^* and lattice constant a using $t \equiv 2\hbar^2/3m^*a^2$. Δ is the spin-orbit coupling.

	m^*	a	t	Δ
MoS_2	0.64	0.312	0.82	0.152
$MoSe_2$	0.70	0.325	0.69	0.196
WS_2	0.49	0.313	1.06	0.425
WSe_2	0.54	0.325	0.89	0.463

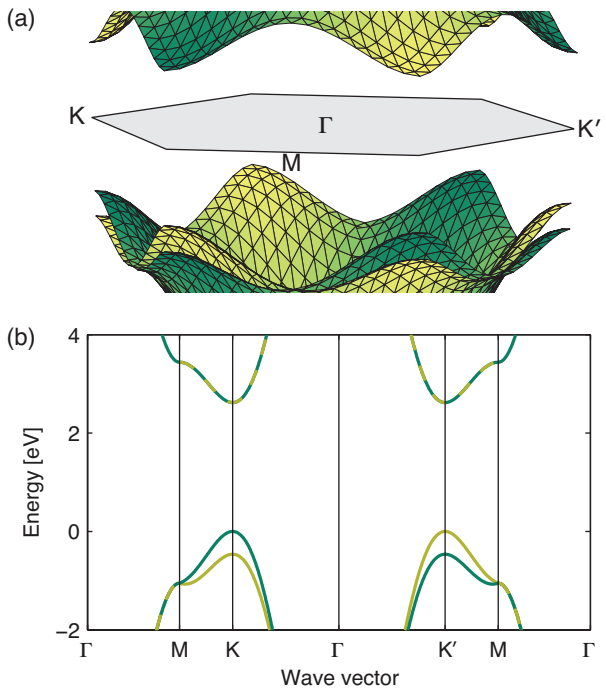

FIG. 2. (Color online) (a) The electron band structure of the minimalistic lattice model captures the band gap, band curvature, and valence-band split at the K and K′ points. (b) Additional parameters are needed for other band features such as a spin-split conduction band and a valence band with a local maximum at Γ near its band edge. Bright and dark curves indicate spin. Parameters: $E_g = 2.6$ eV, $t = 0.89$ eV, and $\Delta = 0.463$ eV.

are concentrated around the corners of the hexagonal Brillouin zone,[8] at the symmetry points K and K′, shown in Fig. 1(c). These symmetry points are located at $\vec{K}_\tau = 4\pi\tau\hat{x}/3a$ with $\tau \in \{\pm 1\}$ being a valley index. At these symmetry points, the d-orbitals in the conduction and valence bands take the form d_{z^2} and $d_{x^2-y^2} \pm id_{xy}$, respectively, which are shown in Fig. 1(d). These orbitals are generally hybridized[34,35,37] throughout the Brillouin zone. This hybridization can be ignored, however, so long as we restrict the usage of our model to an energy regime near the band edges. With this restriction in mind, we shall herein treat the the conduction and valence band as two non-interacting bands. We also restrict the interaction between different localized Wannier orbitals to nearest neighbors, which relative to an arbitrary site are located at the six sites $\vec{\delta} \in \{\pm\vec{a}_1, \pm\vec{a}_2, \pm(\vec{a}_1 - \vec{a}_2)\}$. The Hamiltonian could then be expressed as $\hat{H} = \sum_{n\sigma} \hat{H}_{n\sigma}$ with

$$\hat{H}_{n\sigma} = \sum_{\vec{R}\vec{\delta}} t_{n\sigma\vec{\delta}} c^\dagger_{n\sigma\vec{R}+\vec{\delta}} c_{n\sigma\vec{R}} + \sum_{\vec{R}} \varepsilon_n c^\dagger_{n\sigma\vec{R}} c_{n\sigma\vec{R}}, \tag{2}$$

where $t_{n\sigma\vec{\delta}}$ and ε_n are nearest-neighbor and onsite hopping parameters, respectively. In the absence of the spin-orbit interaction, $t_{n\sigma\vec{\delta}}$ is spin-independent and isotropic. The latter isotropy is evident from the lack of azimuthal dependence of the magnitude of the d-orbitals in Fig. 1(d). To account for the spin-orbit interaction, which is significant in the transition

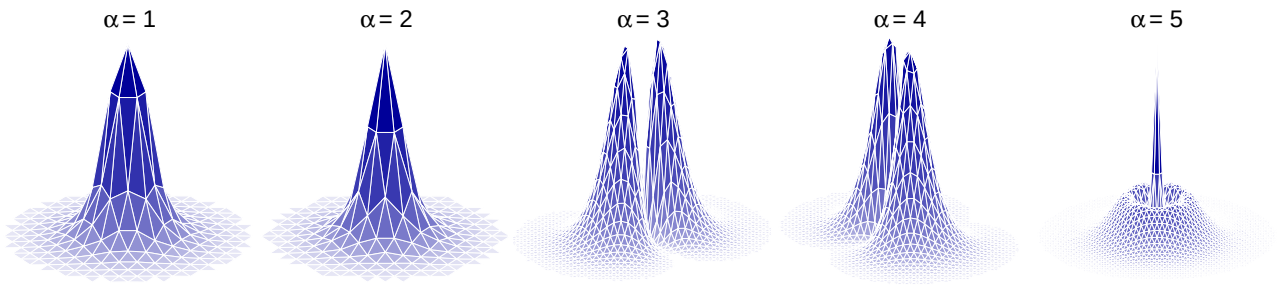

FIG. 3. (Color online) Real-space probability density $|\xi_{\sigma\vec{K}\alpha\vec{R}}|^2$ of the electron for a centered hole in zone-center exciton states. The triangular lattice grid shows that the electron and hole in the $\alpha = 1$ ($1s$-A) and $\alpha = 2$ ($1s$-B) exciton states are tightly bound and are likely to be found on the same or neighboring sites. Parameters: $t = 0.89$ eV, $\Delta = 0.463$ eV, $\varepsilon_r = 3.2$ and $\Delta v_0 = 1.6$ eV.

metals, we add an imaginary term so that

$$t_{n\sigma\vec{\delta}} = t_n + 4i\sigma\tilde{t}_n \sin\vec{K}_+ \cdot \vec{\delta}, \tag{3}$$

where t_n and $\tilde{t}_n$ are real parameters. We have determined the introduced parameters above, up to an arbitrary reference energy, from the band gap E_g, the effective mass m^*, and the spin-orbit coupling Δ:

$$\begin{array}{lll} \varepsilon_c = 3t + E_g & t_c = t & \tilde{t}_c = 0, \\ \varepsilon_v = -3t - \Delta/2 & t_v = -t & \tilde{t}_v = \Delta/18, \end{array} \tag{4}$$

where $t \equiv 2\hbar^2/3m^*a^2$, and the band indices c and v refer to the the conduction and valence band, respectively.

The single-particle band structure

$$\varepsilon_{n\sigma\vec{k}} = \varepsilon_n + \sum_{\vec{\delta}} t_{n\sigma\vec{\delta}} e^{-i\vec{k}\cdot\vec{\delta}}, \tag{5}$$

is shown in Fig. 2 for tungsten diselenide (WSe_2). Parameters for additional semiconducting transition metal dichalcogenides are provided in Table I.

III. TRIANGULAR LATTICE EXCITON MODEL

When dealing with elementary excitations, it is convenient to perform a canonical transformation that takes into account electrons in the conduction band and holes in the valence band. Consider an elementary excitation bringing an electron with spin σ from a state in the valence band with wave vector $\vec{k}_v = \vec{k} - \vec{K}/2$ across the band gap into a state in the conduction band with wave vector $\vec{k}_c = \vec{k} + \vec{K}/2$. This excitation creates an electron with $\vec{k}_e = \vec{k}_c$ and a hole with $\vec{k}_h = -\vec{k}_v$ so that the combined wave vector becomes $\vec{K}$. This combined wave vector commutes with the Hamiltonian and is therefore a good quantum number. Other quantum numbers are σ and λ, the latter describing the relative motion of the electron and hole. Defining the phase-modified annihilation operators

$$\tilde{c}_{\sigma\vec{R}} = c_{c\sigma\vec{R}} e^{-i\vec{K}\cdot\vec{R}/2}, \tag{6a}$$

$$\tilde{d}_{\bar{\sigma}\vec{R}} = \sigma c^\dagger_{v\sigma\vec{R}} e^{-i\vec{K}\cdot\vec{R}/2}, \tag{6b}$$

for an electron and hole, respectively, we can express a general excitation state as

$$|\mathrm{exc}\rangle = \frac{1}{\sqrt{N}} \sum_{\vec{R}\vec{R}'} \xi_{\sigma\vec{K}\lambda\vec{R}} \tilde{c}^\dagger_{\sigma\vec{R}'+\vec{R}} \tilde{d}^\dagger_{\bar{\sigma}\vec{R}'} |0\rangle, \tag{7}$$

where N is the number of lattice sites, $\xi_{\sigma\vec{K}\lambda\vec{R}}$ is the direct space eigenfunction for the electron/hole pair, and $|0\rangle$ is the vacuum state. The focus below is to obtain $\xi_{\sigma\vec{K}\lambda\vec{R}}$ by solving for the relative motion of the electron and hole.

The Hamiltonian $\hat{H}$ describing the electron-hole pair contains a mutual Coulomb interaction as well as the single-particle contributions described above. We neglect Coulomb contributions from electrons in the valence bands and approximate the screened Coulomb integrals as

$$V_{\vec{R}} \equiv \begin{cases} \frac{e^2}{4\pi\varepsilon_r\varepsilon_0|\vec{R}|} & (\vec{R} \neq 0), \\ \Delta v_0 & (\vec{R} = 0), \end{cases} \tag{8}$$

where e is the elementary charge, ε_0 is the vacuum permittivity, and $\Delta v_0 \equiv v_0 - w_0$ is the difference between the direct integral v_0, and the exchange integral w_0, the latter assumed to be negligible when the electron and hole occupy different sites.

In analogy with the hydrogen atom, we choose the origin to be position of the positive charge carrier, in this case, the hole. We also let this origin track the motion of the hole, thereby transfering the kinetic energy of the hole over to the electron. This allows us to express the hole-centered electron/hole pair Hamiltonian as

$$\hat{H}_{\sigma\vec{K}} = \sum_{\vec{R}\vec{\delta}} T_{\sigma\vec{K}\vec{\delta}} \tilde{c}^\dagger_{\sigma\vec{R}+\vec{\delta}} \tilde{c}_{\sigma\vec{R}} + \sum_{\vec{R}} (E_0 - V_{\vec{R}}) \tilde{c}^\dagger_{\sigma\vec{R}} \tilde{c}_{\sigma\vec{R}}, \tag{9}$$

where the coefficients

$$T_{\sigma\vec{K}\vec{\delta}} \equiv t_{c\sigma\vec{\delta}} e^{-i\vec{K}\cdot\vec{\delta}/2} - t_{v\sigma\vec{\delta}} e^{i\vec{K}\cdot\vec{\delta}/2}, \tag{10a}$$

$$E_0 \equiv \varepsilon_c - \varepsilon_v - E_g, \tag{10b}$$

can be obtained from Eqs. (3) and (4) with parameters from Table I.

The solutions of the characteristic equation for the relative motion

$$\hat{H}_{\sigma\vec{K}} |\sigma\vec{K}\lambda\rangle = E_{\sigma\vec{K}\lambda} |\sigma\vec{K}\lambda\rangle \tag{11}$$

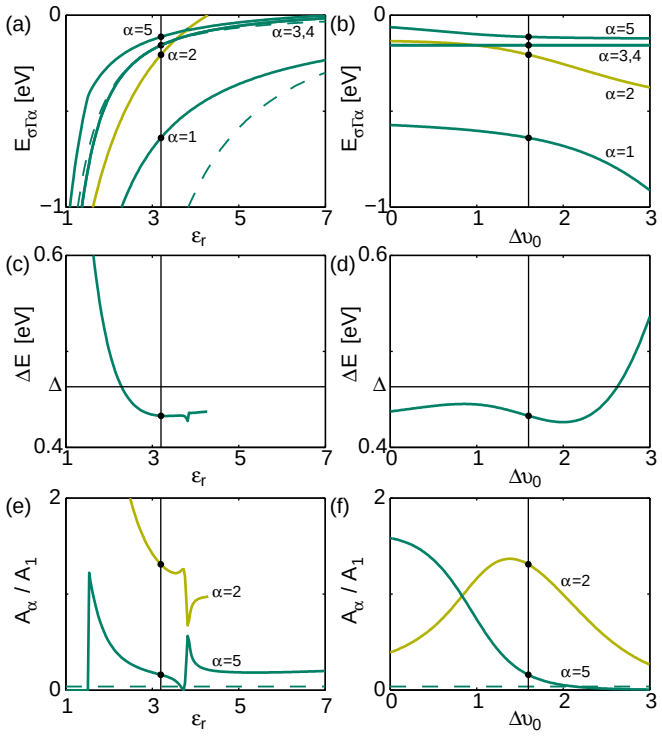

FIG. 4. (Color online) Zone-center excitons. Exciton energy as a function of the relative permittivity (a) and onsite Coulomb interaction (b) with the intersection $\varepsilon_r = 3.2$ and $\Delta v_0 = 1.6$ indicated by vertical lines. Solid and dashed curves obtained from the 3-ALE model and the the 2D hydrogen model, respectively. While there is good agreement for the $\alpha = 3, 4$ ($2p$) curve, the latter model breaks down for the tightly bound electron/hole pairs in the $\alpha = 1$ ($1s$–A) and $\alpha = 2$ ($1s$–B) states. The energy separation between these states depends on the relative permittivity (c) and onsite Coulomb interaction (d), as well as the spin-orbit coupling Δ. The oscillator strengths relative to that of $\alpha = 1$ ($1s$–A) are shown in (e) and (f). Dark and bright curves represent exciton states from the A series and B series, respectively. Additional parameters: $t = 0.89\,\text{eV}$ and $\Delta = 0.463\,\text{eV}$.

provide the electron/hole pair eigenenergies $E_{\sigma\vec{K}\lambda}$ and eigenstates of the form

$$|\sigma\vec{K}\lambda\rangle = \sum_{\vec{R}} \xi_{\sigma\vec{K}\lambda\vec{R}} \tilde{c}^{\dagger}_{\sigma\vec{R}} |0\rangle. \tag{12}$$

These states can be divided into two sets: (1) bound electron/hole-pair states known as excitons and (2) unbound electron/hole-pair states. The former states appear at discrete energies and are described by $\lambda = \alpha$, where we let α take positive integers counted from the strongest bound state. The latter unbound states are continuous in energy and are described by $\lambda = \vec{k}$.

TABLE II. Hydrogen shell labels for the lowest five quantum numbers describing excitations from the valence band (Series A) and split-off band (Series B) resulting from the spin-orbit coupling.

Quantum number	$\alpha = 1$	$\alpha = 2$	$\alpha = 3$	$\alpha = 4$	$\alpha = 5$
Series A label	$1s$		$2p_x$	$2p_y$	$2s$
Series B label		$1s$			

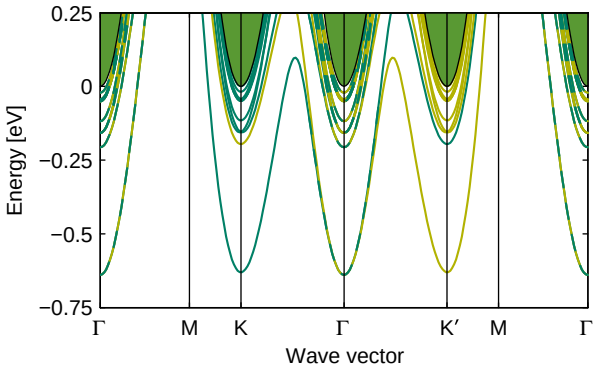

FIG. 5. (Color online) Electron/hole pair band structure. Discrete bands and filled regions contain bound exciton states and free electron/hole pairs, respectively. Bright and dark bands indicate spin of the excited electron. The bands, enumerated at Γ starting from the strongest bound state, are: $\alpha = 1$ ($1s$–A), $\alpha = 2$ ($1s$–B), $\alpha = 3, 4$ ($2p$), and $\alpha = 5$ ($2s$). Parameters: $t = 0.89\,\text{eV}$, $\Delta = 0.463\,\text{eV}$, $\varepsilon_r = 3.2$, and $\Delta v_0 = 1.6\,\text{eV}$.

The exciton states with the wave vector $\vec{K}$ at the zone center Γ are of particular importance for optoelectronic experiments due to the relative high speed of light causing almost vertical electronic excitations. The eigenfunctions of the five strongest bound Γ excitons are shown in Fig. 3, where each vertex represents a transition metal lattice site. Strictly, the lattice symmetry prohibits the exciton quantum numbers α from being separated into radial and azimuthal quantum numbers. For the lowest-energy bands, however, designation using shell labels from the hydrogen model still makes sense and we provide the conversion in Table II.

The exciton energies depend on the screened Coulomb interaction, as depicted in Fig. 4. First, we note that the $\alpha = 3, 4$ ($2p$) curves are lower in energy than the $\alpha = 5$ ($2s$) curve, in agreement with first-principles predictions.[16] Second, we note that the $\alpha = 2$ ($1s$–B) exciton only appears below the band edge for a sufficiently small dielectric constant. In this regime, the hydrogen model also breaks down for the A exciton series due to the tightly bound electron/hole pairs. Third, the $\alpha = 3, 4$ ($2p$) states have a node at the origin and are unaffected by Δv_0. Fourth, the energy separation between the $\alpha = 1$ and $\alpha = 2$ states ("the well-known A-B exciton split") is not only a function of the spin-orbit coupling but also the Coulomb interaction. Fifth, the Coulomb interaction also affects the relative oscillator strengths $A_\alpha/A_1 \equiv |\xi_{\sigma\vec{0}\alpha\vec{0}}|^2/|\xi_{\sigma\vec{0}1\vec{0}}|^2$ and could be modulated through the dielectric environment.

Exciton states away from the zone center could also potentially be exploited in applications. The energies of these states, $E_{\sigma\vec{K}\alpha}$, are shown as discrete bands in Fig. 5. Reflection symmetry or time-reversal symmetry causes the zone-center states to be doubly degenerate and requires the K excitons to have the same energies as the K′ excitons with the opposite excited spin.[38,39] This degeneracy could be broken, however, by an external magnetic field.[40,41] Transitions between exciton

states are possible through additional interactions, as long as they exhibit appropriate symmetry.[42,43] First-principles band structures indicate that there might be additional states near K and K′ originating from the valence band Γ point. To capture these states, the single-particle basis would need to be expanded.

The electron/hole pair band structure also contains unbound states. Unbound states have been derived analytically for the 2D hydrogen model.[10] Obtaining similar solutions using the 3-ALE model is not practical, owing to the large number of sites needed for such calculations. Therefore, we model instead the filled regions in Fig. 5 using free electron/hole pairs. For these free electron/hole pairs, the Coulomb interaction $v_{\vec{R}} \to 0$. The eigenfunctions are then Bloch waves given by $\xi_{\sigma\vec{K}\vec{k}\vec{R}} = N^{-1/2}\, e^{i\vec{k}\cdot\vec{R}}$. The corresponding energies of the free electron/hole pairs are

$$E_{\sigma\vec{K}\vec{k}} = E_0 + \sum_{\vec{\delta}} t_{\sigma\vec{K}\vec{\delta}}\, e^{-i\vec{k}\cdot\vec{\delta}}, \tag{13}$$

where we have as expected $E_{\bar{\sigma}\vec{K}\vec{k}} = E_{\sigma-\vec{K}-\vec{k}}$, again from time-reversal symmetry.

IV. CONCLUSIONS

The model presented herein have been derived from the many-body Hamiltonian with the goal to extract the dominant physics among the elementary excitations in 2D semiconductors with a equilateral triangular lattice. The approximations should be reasonable for tightly bound electron/hole pairs, and we therefore expect the model to work well for optically driven transitions into the lower exciton states. The predicted results are in qualitative agreement with first-principles quasiparticle calculations, and for improved accuracy, we suggest using this model with a more detailed dielectric environment with a complex dielectric function that is spatially[44] and/or energy dependent.[45,46] To achieve a better description away from the band edges, which could be needed for zone-corner excitons, it is also recommended to use a larger basis to account for d-band hybridization.[37,47,48] During the final stage of this paper, the authors have become aware of a recent paper including such hybridization effects for excitons in MoS_2.[49]

In summary, we have presented a minimalistic and computationally efficient model capturing the essential physics of low-energy electronic excitations. This model could be used to understand experimental absorption spectra and is well suited to serve as a foundation for more advanced models, which could describe exciton coupling to, e.g., defects, interfaces, vibrations, and externally applied fields.

ACKNOWLEDGMENTS

This work has been supported by the Office of Naval Research (ONR), directly and through the Naval Research Laboratory (NRL). The authors thank Brett Dunlap, Ergun Simsek, and Carter White for discussions. F. T. acknowledges support from NRL through the National Research Council (NRC) Research Associateship Program.

* daniel.gunlycke@nrl.navy.mil
† National Research Council Research Associate

[1] J. Frenkel, "On the transformation of light into heat in solids. i," Phys. Rev. **37**, 17 (1931).
[2] G. H. Wannier, "The structure of electronic excitation levels in insulating crystals," Phys. Rev. **52**, 0191 (1937).
[3] R. F. Friend and A. D. Yoffe, "Physical properties of layer structures - optical properties and photoconductivity of thin crystals of molybdenum disulphide," Proc. R. Soc. A **273**, 69 (1963).
[4] B. L. Evans and P. A. Young, "Optical absorption and dispersion in molybdenum disulphide," Proc. R. Soc. A **284**, 402 (1965).
[5] J. A. Wilson and A. D. Yoffe, "Transition metal dichalcogenides discussion and interpretation of observed optical, electrical and structural properties," Adv. Phys. **18**, 193 (1969).
[6] K. S. Novoselov, D. Jiang, F. Schedin, T. J. Booth, V. V. Khotkevich, S. V. Morozov, and A. K. Geim, "Two-dimensional atomic crystals," Proc. Nat. Acad. Sci. USA **102**, 10451 (2005).
[7] T. S. Li and G. L. Galli, "Electronic properties of mos2 nanoparticles," J. Phys. Chem. C **111**, 16192 (2007).
[8] K. F. Mak, C. Lee, J. Hone, J. Shan, and T. F. Heinz, "Atomically thin mos2: A new direct-gap semiconductor," Phys. Rev. Lett. **105**, 136805 (2010).
[9] H. I. Ralph, "The electronic absorption edge in layer type crystals," Solid State Commun. **3**, 303 (1965).
[10] M. Shinada and S. Sugano, "Interband optical transitions in extremely anisotropic semiconductors. i. bound and unbound exciton absorption," J. Phys. Soc. Jpn **21**, 1936 (1966).
[11] A. Molina-Sanchez and L. Wirtz, "Phonons in single-layer and few-layer mos2 and ws2," Phys. Rev. B **84**, 155413 (2011).
[12] T. Cheiwchanchamnangij and W. R. L. Lambrecht, "Quasiparticle band structure calculation of monolayer, bilayer, and bulk mos2," Phys. Rev. B **85**, 205302 (2012).
[13] Y. X. Lin, X. Ling, L. L. Yu, S. X. Huang, A. L. Hsu, Y. H. Lee, J. Kong, M. S. Dresselhaus, and T. Palacios, "Dielectric screening of excitons and trions in single-layer mos2," Nano Lett. **14**, 5569 (2014).
[14] A. R. Beal and W. Y. Liang, "Excitons in 2h-wse2 and 3r-ws2," J. Phys. C **9**, 2459 (1976).
[15] A. Chernikov, T. C. Berkelbach, H. M. Hill, A. Rigosi, Y. L. Li, O. B. Aslan, D. R. Reichman, M. S. Hybertsen, and T. F. Heinz, "Exciton binding energy and nonhydrogenic rydberg series in monolayer ws2," Phys. Rev. Lett. **113**, 076802 (2014).
[16] Z. L. Ye, T. Cao, K. O'Brien, H. Y. Zhu, X. B. Yin, Y. Wang, S. G. Louie, and X. Zhang, "Probing excitonic dark states in single-layer tungsten disulphide," Nature **513**, 214 (2014).
[17] K. L. He, N. Kumar, L. Zhao, Z. F. Wang, K. F. Mak, H. Zhao, and J. Shan, "Tightly bound excitons in monolayer wse2," Phys. Rev. Lett. **113**, 026803 (2014).
[18] A. T. Hanbicki, M. Currie, G. Kioseoglou, A. L. Friedman, and B. T. Jonker, "Measurement of high exciton binding energy in the monolayer transition-metal dichalcogenides ws2 and wse2," Solid State Commun. **203**, 16 (2015).

[19] B. Zhu, X. Chen, and X. Cui, "Exciton binding energy of monolayer ws2," Sci. Rep. **5**, 9218 (2015).

[20] A. Kumar and P. K. Ahluwalia, "Electronic structure of transition metal dichalcogenides monolayers 1h-mx2 (m = mo, w; x = s, se, te) from ab-initio theory: new direct band gap semiconductors," Eur. Phys. J. B **85**, 186 (2012).

[21] A. Ramasubramaniam, "Large excitonic effects in monolayers of molybdenum and tungsten dichalcogenides," Phys. Rev. B **86**, 115409 (2012).

[22] H. L. Shi, H. Pan, Y. W. Zhang, and B. I. Yakobson, "Quasiparticle band structures and optical properties of strained monolayer mos2 and ws2," Phys. Rev. B **87**, 155304 (2013).

[23] W. Q. Li, C. F. J. Walther, A. Kuc, and T. Heine, "Density functional theory and beyond for band-gap screening: Performance for transition-metal oxides and dichalcogenides," J. Chem. Theo. Comp. **9**, 2950 (2013).

[24] Y. F. Liang, S. T. Huang, R. Soklaski, and L. Yang, "Quasiparticle band-edge energy and band offsets of monolayer of molybdenum and tungsten chalcogenides," Appl. Phys. Lett. **103**, 042106 (2013).

[25] D. Y. Qiu, F. H. da Jornada, and S. G. Louie, "Optical spectrum of mos2: Many-body effects and diversity of exciton states," Phys. Rev. Lett. **111**, 216805 (2013).

[26] R. Soklaski, Y. F. Liang, and L. Yang, "Temperature effect on optical spectra of monolayer molybdenum disulfide," Appl. Phys. Lett. **104**, 193110 (2014).

[27] Y. F. Liang, R. Soklaski, S. T. Huang, M. W. Graham, R. Havener, J. Park, and L. Yang, "Strongly bound excitons in gapless two-dimensional structures," Phys. Rev. B **90**, 115418 (2014).

[28] A. R. Klots, A. K. M. Newaz, B. Wang, D. Prasai, H. Krzyzanowska, J. H. Lin, D. Caudel, N. J. Ghimire, J. Yan, B. L. Ivanov, K. A. Velizhanin, A. Burger, D. G. Mandrus, N. H. Tolk, S. T. Pantelides, and K. I. Bolotin, "Probing excitonic states in suspended two-dimensional semiconductors by photocurrent spectroscopy," Sci. Rep. **4**, 6608 (2014).

[29] M. M. Ugeda, A. J. Bradley, S. F. Shi, F. H. da Jornada, Y. Zhang, D. Y. Qiu, W. Ruan, S. K. Mo, Z. Hussain, Z. X. Shen, F. Wang, S. G. Louie, and M. F. Crommie, "Giant bandgap renormalization and excitonic effects in a monolayer transition metal dichalcogenide semiconductor," Nat. Mater. **13**, 1091 (2014).

[30] F. Fuchs, C. Rodl, A. Schleife, and F. Bechstedt, "Efficient o(n(2)) approach to solve the bethe-salpeter equation for excitonic bound states," Phys. Rev. B **78**, 085103 (2008).

[31] G. Berghauser and E. Malic, "Analytical approach to excitonic properties of mos2," Phys. Rev. B **89**, 125309 (2014).

[32] S. Konabe and S. Okada, "Effect of coulomb interactions on optical properties of monolayer transition-metal dichalcogenides," Phys. Rev. B **90**, 155304 (2014).

[33] F. Huser, T. Olsen, and K. S. Thygesen, "How dielectric screening in two-dimensional crystals affects the convergence of excited-state calculations: Monolayer mos2," Phys. Rev. B **88**, 245309 (2013).

[34] L. F. Mattheiss, "Energy-bands for 2h-nbse2 and 2h-mos2," Phys. Rev. Lett. **30**, 784 (1973).

[35] L. F. Mattheiss, "Band structures of transition-metal-dichalcogenide layer compounds," Phys. Rev. B **8**, 3719 (1973).

[36] R. Coehoorn, C. Haas, J. Dijkstra, C. J. F. Flipse, R. A. Degroot, and A. Wold, "Electronic-structure of mose2, mos2, and wse2. 1. band-structure calculations and photoelectron-spectroscopy," Phys. Rev. B **35**, 6195 (1987).

[37] G. B. Liu, W. Y. Shan, Y. G. Yao, W. Yao, and D. Xiao, "Three-band tight-binding model for monolayers of group-vib transition metal dichalcogenides," Phys. Rev. B **88**, 085433 (2013).

[38] W. Yao, D. Xiao, and Q. Niu, "Valley-dependent optoelectronics from inversion symmetry breaking," Phys. Rev. B **77**, 235406 (2008).

[39] D. Xiao, G. B. Liu, W. X. Feng, X. D. Xu, and W. Yao, "Coupled spin and valley physics in monolayers of mos2 and other group-vi dichalcogenides," Phys. Rev. Lett. **108**, 196802 (2012).

[40] Y. L. Li, J. Ludwig, T. Low, A. Chernikov, X. Cui, G. Arefe, Y. D. Kim, A. M. van der Zande, A. Rigosi, H. M. Hill, S. H. Kim, J. Hone, Z. Q. Li, D. Smirnov, and T. F. Heinz, "Valley splitting and polarization by the zeeman effect in monolayer mose2," Phys. Rev. Lett. **113**, 266804 (2014).

[41] D. MacNeill, C. Heikes, K. F. Mak, Z. Anderson, A. Kormanyos, V. Zolyomi, J. Park, and D. C. Ralph, "Breaking of valley degeneracy by magnetic field in monolayer mose2," Phys. Rev. Lett. **114**, 037401 (2015).

[42] Y. Song and H. Dery, "Transport theory of monolayer transition-metal dichalcogenides through symmetry," Phys. Rev. Lett. **111**, 026601 (2013).

[43] M. M. Glazov, T. Amand, X. Marie, D. Lagarde, L. Bouet, and B. Urbaszek, "Exciton fine structure and spin decoherence in monolayers of transition metal dichalcogenides," Phys. Rev. B **89**, 201302 (2014).

[44] T. C. Berkelbach, M. S. Hybertsen, and D. R. Reichman, "Theory of neutral and charged excitons in monolayer transition metal dichalcogenides," Phys. Rev. B **88**, 045318 (2013).

[45] Y. L. Li, A. Chernikov, X. Zhang, A. Rigosi, H. M. Hill, A. M. van der Zande, D. A. Chenet, E. M. Shih, J. Hone, and T. F. Heinz, "Measurement of the optical dielectric function of monolayer transition-metal dichalcogenides: Mos2, mose2, ws2, and wse2," Phys. Rev. B **90**, 205422 (2014).

[46] B. Mukherjee, F. Tseng, D. Gunlycke, K. K. Amara, G. Eda, and E. Simsek, "Complex electrical permittivity of the monolayer molybdenum disulfide (mos2) in near uv and visible," Opt. Mat. Express **5**, 447 (2015).

[47] F. Zahid, L. Liu, Y. Zhu, J. Wang, and H. Guo, "A generic tight-binding model for monolayer, bilayer and bulk mos2," AIP Adv. **3**, 052111 (2013).

[48] E. Cappelluti, R. Roldan, J. A. Silva-Guillen, P. Ordejon, and F. Guinea, "Tight-binding model and direct-gap/indirect-gap transition in single-layer and multilayer mos2," Phys. Rev. B **88**, 075409 (2013).

[49] F. C. Wu, F. Y. Qu, and A. H. MacDonald, "Exciton band structure of monolayer mos2," Phys. Rev. B **91**, 075310 (2015).